Published in final edited form as:
Biochemistry. 2009 June 23; 48(24): 5573–5581. doi:10.1021/bi900325k.

The Loop Connecting Metal-Binding Domains 3 and 4 of ATP7B Is a Target of a Kinase-Mediated Phosphorylation†

Mee Y. Bartee, **Martina Ralle**, and **Svetlana Lutsenko***
Department of Biochemistry and Molecular Biology, Oregon Health and Science University, Portland, Oregon 97239

Abstract

Cu-ATPase ATP7B (Wilson's disease protein) transports copper into the trans-Golgi network for biosynthetic incorporation into ceruloplasmin and sequesters excess copper to endocytic vesicles for further export out of the cell. The activity and intracellular location of ATP7B are regulated by copper levels; the trafficking of ATP7B between cellular compartments is coupled to changes in the level of protein phosphorylation. Neither the nature of the kinase(s) phosphorylating ATP7B nor the location of phosphorylation sites is known. We demonstrate that the membrane-bound ATP7B is phosphorylated by an ATP-dependent, GTP-independent kinase that can be either soluble or membrane-associated. Mg^{2+} or Mn^{2+} is necessary for kinase activity. We further show that the recombinant N-terminal domain of ATP7B (N-ATP7B) is a specific target for a kinase-mediated phosphorylation in vitro and in cells. Although exogenous addition of copper is not required for kinase activity, copper binding to N-ATP7B markedly alters the exposure of loops connecting the metal-binding subdomains (MBDs) to proteolysis and facilitates phosphorylation by 25–30%. MBD1–2 and MBD4–5 linkers become protected, while MBD2–3 and MBD3–4 regions remain exposed. A significant, 5-fold increase in the level of phosphorylation is also observed for the ATP7B variant that lacks the 29 kDa N-terminal fragment (mostly likely comprised of MBD1–3). Analysis of phosphorylated peptides by two-dimensional gel electrophoresis and mass spectrometry points to the loop connecting MBD3 andMBD4 as a region of phosphorylation. Altogether, the results suggest a mechanism in which kinase-mediated phosphorylation of ATP7B is controlled by a conformational state of N-ATP7B.

Cu-ATPase ATP7B[1] plays an essential role in human copper metabolism. ATP7B is expressed in the liver, a major copper homeostatic organ in the body, where it performs two functions. Under basal conditions, ATP7B resides in the trans-Golgi network (TGN), where it transports copper from the cytosol to the TGN lumen for incorporation into ceruloplasmin, a copper-

†This work was supported by National Institutes of Health Grants R01 DK071865 and P01 GM067166 to S.L. M.Y.B. (Min) was a recipient of NRSA Fellowship F31NS047963.

*To whom correspondence should be addressed: Department of Biochemistry and Molecular Biology, Oregon Health and Science University, 3181 SW Sam Jackson Park Rd., Portland, OR 97239-3098. Telephone: (503) 494-6953. Fax: (503) 494-8393. lutsenko@ohsu.edu.

SUPPORTING INFORMATION AVAILABLE

Potential tryptic target sites were identified using the PAWS program. Fragments cleaving the loop regions and leaving individual MBDs intact, except for MBD5–6 which contains a very short linker, were used to calculate the isoelectric points for the fragments with and without a phosphate in SEQUEST. The values were plotted, molecular mass versus theoretical pI, in SigmaPlot. This material is available free of charge via the Internet at http://pubs.acs.org.

[1]Abbreviations: ATP7B, Wilson's disease protein; N-ATP7B, N-terminal ATP7B; MBD, metal-binding domain; 2D, two-dimensional; TGN, trans-Golgi network; ABD, ATP-binding domain; ATP7A, Menkes disease protein; *Sf9*, *Spodoptera frugiperda*; HB, homogenization buffer; PB, phosphorylation buffer; MBP-N-ATP7B, N-terminal ATP7B maltose-binding protein fusion; CBD, chitin binding domain; His-N-ATP7B, His-tagged N-terminal ATP7B; pI, isoelectric point.

dependent ferroxidase. When the hepatic level of copper becomes elevated, ATP7B traffics from the TGN to vesicles in the vicinity of the apical plasma membrane (1–4). ATP7B sequesters excess copper into the vesicles; the vesicles then fuse with the apical membrane, and excess copper is exported. When copper levels are normalized, ATP7B returns back to the TGN. Thus, the relocalization of ATP7B in response to copper level elevation is central to the regulation of copper levels in the liver. This process depends on the ability of ATP7B to sense changing copper concentrations and be recognized by the components of cellular trafficking machinery. The biochemical mechanism that couples cellular copper elevation and ATP7B trafficking remains poorly understood.

ATP7B is a large 165 kDa membrane protein with several cytosolic domains (Figure 1) (5). The N-terminal domain of ATP7B (N-ATP7B) has six metal-binding subdomains (MBD); each MBD binds one Cu(I) atom (6). Binding of copper to N-ATP7B is accompanied by conformational changes [as evidenced by CD spectroscopy measurements (7)], making this region a likely candidate for the role of a copper sensor. It has also been shown that copper binding to N-ATP7B weakens interactions between N-ATP7B and the ATP-binding domain of ATP7B (ABD) (8) and that the deletion of the N-terminal region, including the first four MBDs (MBD1–4), increases the rate of ATP hydrolysis byATP7B (9). Altogether, these observations led to the model in which the MBD1–4 in the apo form acts as an autoinhibitory domain downregulating the Cu-ATPase activity, and the interaction between N-ATP7B and ABD protects sites that are recognized by the components of trafficking machinery. Copper binding to regulatory MBD1–4 stimulates copper transport by ATP7B and presumably facilitates the trafficking of the transporter by exposing sites for further modifications and protein–protein interactions (Figure 1).

In cells, ATP7B undergoes a kinase-mediated phosphorylation and the level of phosphorylation is regulated by copper (10). At low levels of copper, ATP7B has a basal level of phosphorylation regardless of whether N-ATP7B is present. At elevated levels of copper, ATP7B becomes hyperphosphorylated (this response requires the presence of N-ATP7B) (10). Hyperphosphorylation is associated with the relocalization of ATP7B from the TGN to vesicles, while the return of ATP7B from vesicles to the TGN is accompanied by dephosphorylation. Different sensitivity of basal and copper-dependent phosphorylation to treatment with λ-phosphatase (10) suggested that at least two different sites are phosphorylated, possibly by different kinases. The ATP7B homologue, ATP7A, undergoes similar phosphorylation in response to copper (11), suggesting that kinase-mediated phosphorylation is a common mechanism for regulating the intracellular localization of human Cu-ATPases. To identify the molecular and mechanistic link between phosphorylation and trafficking, it is important to establish the location of the phosphorylation sites and characterize the kinase(s) phosphorylating Cu-ATPases.

In this study, we developed conditions for in vitro phosphorylation of ATP7B, demonstrated that N-ATP7B is a target of kinase-mediated phosphorylation in vitro and in vivo, and identified regions that undergo conformational transitions in response to copper binding. We further showed that the loop between MBD3 and -4, which remains exposed upon copper binding, becomes a target of a kinase-mediated phosphorylation. On the basis of our data, we propose a working model of how elevation of the level of copper may trigger kinase-mediated phosphorylation and trafficking response of ATP7B.

MATERIALS AND METHODS

Culturing Sf9 Cells

Sf9 cells were cultured in Ex-Cell 420 media (JRH Biosciences Inc.) in spinner flasks (BellCo, Vineland, NJ) onmagnetic stir plates with constant aeration. The cells were kept at 27 °C in

ambient air. For expression ofATP7B, 1×10^6 cells/mL were infected with baculovirus expressing either control ATP7B, the catalytically inactive D^{1027} A mutant of ATP7B, or their His-tagged variants, for 72 h before harvesting of membranes. Mock infection with empty virus, AvMNPV, was performed as a control. *Sf9* cells were homogenized on ice using a tight fit dounce homogenizer (Wheaton Science Products, Millville, NJ) in homogenization buffer (HB) [25 mM imidazole (pH 7.5), 250 mM sucrose, 1 mM DTT, 2 mM 4-(2-aminoethyl) benzenesulfonyl fluoride hydrochloride (AEBSF), and one EDTA free Protease Inhibitor Cocktail tablet per 250 mL of cells (Roche Pharmaceuticals, Nutley, NJ)]. To remove cell debris, the homogenate was centrifuged for 10 min at 500*g* (4 °C), and the supernatant was transferred into fresh tubes. Microsomal membranes were then pelleted at 20000*g* for 30 min (4 °C), and the supernatant was discarded. Membranes were resuspended in HB. The protein concentration in membrane preparations was determined by the Lowry method (12), and the ATP7B expression was confirmed by Western blotting using the anti-N-ATP7B antibody. Aliquots of membrane protein were stored at −80 °C until they were needed. Freezing and thawing of samples were minimized to prevent degradation and loss of activity.

In Vitro Phosphorylation of Recombinant ATP7B Expressed in Sf9 Membranes

Sf9 membrane protein (50 μg), isolated as described above, was resuspended in 195 μL of phosphorylation buffer (PB) [20 mM Bis-Tris propane (pH 7.5), 200 mM KCl, 5 mM $MgCl_2$, 1 mM DTT, 2 mM AEBSF, EDTA free Protease Inhibitor Cocktail (Roche Pharmaceuticals), 1 mM sodium orthovanadate, and 100 μM ATP] and 5 μCi of [γ-^{32}P]ATP (Perkin-Elmer, Fremont, CA) (diluted to a volume of 5 μL in PB) and incubated at room temperature for 30 min. Fifty microliters of 50%TCA (trichloroacetic acid) in 1 mM sodium phosphate was added to stop the reaction. In the experiments shown in Figure 2, the phosphorylation buffer was at pH 6.0 and contained 1 μM ATP (instead of 100 μM in all other experiments). The precipitated proteins were collected by centrifugation at 20000*g* (4 °C). The pellet was rinsed with 1 mL of water and resuspended in Laemmli gel sample buffer containing 2.6 M urea. The proteins were separated with a 7.5% Laemmli gel and then either dried or transferred to the PVDF membrane (Immobilon-P, Millipore, Billerica, MA), and the radioactive bands were detected by autoradiography using Kodak BioMax MS film. To calculate the protein amount in the ATP7B band, PVDF membranes were stained with Commassie Blue and subjected to densitometry using a Bio-Rad Molecular Imager & Analyst. For calculations of the ratio of phosphate to protein, the Coomassie-stained ATP7B bands from PVDF were excised and placed into liquid scintillation cocktail and β-emission was counted using a liquid scintillation counter.

Purification of ATP7B-His Expressed in Sf9 Cells

Sf9 cells were infected with a baculovirus expressing ATP7B with the C-terminal His tag, and membranes were collected as described above. The membranes were solubilized in PB (without DTT) containing 1% dodecyl β-maltoside (DDM) (Sigma, St. Louis, MO) and centrifuged at 20000*g* to remove proteins that did not solubilize. Fifty microliters of Ni-NTA (Qiagen, Germantown, MD) slurry was rehydrated with PBS and then incubated with 50 mM $NiSO_4$ for 1 h before equilibration with HB and 0.01% DDM (without DTT). Solubilized *Sf9* membranes were added to the Ni-NTA slurry and incubated for 1 h at room temperature by the batch method on a rotator. The resin was pelleted and the supernatant removed. To remove nonspecifically interacting proteins, the resin was washed with HB and 0.01% DDM (with no DTT) for 100 slurry volumes. Protein was eluted with PBS, containing 250 mM imidazole, 2 mM AEBSF, EDTA free Protease Inhibitor Cocktail, and 0.1% DDM, and loaded onto a Laemmli gel. Proteins on the gels were stained with Coomassie Blue R-250 or transferred onto PVDF for Western blotting with anti-N-ATP7B antibody.

Phosphorylation of MBP-N-ATP7B

Apo and copper-bound forms of MBP-N-ATP7B were generated as previously described (13). For phosphorylation studies, MBP-N-ATP7B bound to amylose resin (NEB, Ipswich, MA) was washed with PBS, containing EDTA-free protease inhibitors. Then 2 mM AEBSF, 150 μg of the soluble fraction of the HEK293 cell lysate, and 100 μM ATP mixed with 5 μCi of [γ-^{32}P]ATP were added, and the slurry was incubated on a rotator for 30 min at room temperature. The resin was washed with 100 slurry volumes of PBS, 2 mM AEBSF, and EDTA free Protease Inhibitor Cocktail (Roche Pharmaceuticals) and eluted with PBS, containing 200 mM maltose. The eluted protein was resuspended in sample buffer and loaded onto 7.5% Laemmli gels. The gels were subsequently stained with Coomassie Blue R-250, dried on a gel drier, and placed under film (Kodak BioMax MS film) for 18 h and developed. The film was then scanned and analyzed using AlphaInnotech, as well as the gels for protein quantitation and normalization.

2D Gel Electrophoresis

Phosphorylated MBP-N-ATP7B was proteolyzed with trypsin, and the fragments were processed with a PlusOne 2-D Clean-Up kit (Amersham Pharmacia). The pelleted fragments were resuspended in 250 μL of isoelectric focus buffer [8 Mdeionized urea, 2%CHAPS, 5 μL of IPG(Amersham Pharmacia) for the 3–10 nonlinear pH range, and 4.54 μL of 1 M DTT]. Protein was added to an IEF chamber, and a 13 cm IEF pH 3–10 nonlinear strip was placed on top of the protein; 800 μL of Dry Strip cover fluid was added on top of the plastic backing of the IEF strip. Samples were run for 20000–30000 V h (10 h for rehydration of the IEF strip + ~16–18 h for protein focusing). Focused strips were then reduced with 10 mg/mL DTT in Laemmli upper buffer [500 mM Tris (pH 6.8) and 0.4% SDS] on a rotator for 20 min. The IEF strip was removed and placed into 25 mg/mL IAA in Laemmli upper buffer for 20 min. The IEF strip was placed on top of a 15% Laemmli gel with a flat stacking gel, leaving a gap of 0.5 in. at the top. One well for the protein ladder was created, and an additional stacking gel was poured on top of the IEF strip to seal the top of the Laemmli gel. Peptides were transferred onto PVDF and the phosphorylated spots exposed to film. Spots were excised and processed by tandem mass spectroscopy.

Peptide Identification by Mass Spectrometry

The peptides were analyzed by liquid chromatography electrospray ionization tandem mass spectroscopy (LC-MS) using an ion trap mass spectrometer (LCQ Deca XP Plus, Thermo Fisher Corp.). The analysis by LC-MS was performed using 180 μm reversed phase capillary columns packed in house with stable-bond packing material (C18 reversed phase material, 5 mm particle size, 100 Å pore size, ZORBAX, Agilent Technologies). The samples were applied to the column through a trap column (180 μm × 2.5 cm, packed in house with the same packing material) and the peptides separated using a linear gradient changing the solvent composition from 2 to 30% acetonitrile over a 30 min period with a constant flow rate of 1.8 μL/min (supplied by an Agilent Cap Pump 1100, Agilent Technologies). MS data were acquired in data-dependent mode in which a single survey scan (MS) is followed by up to four sequential data-dependent MS/MS scans for the four most intense peptide ions. A dynamic exclusion feature was used to extend the analysis to less abundant ions. The peptides were identified with SEQUEST (2). Further validation was performed manually using ProteinProphet (4) and PeptideProphet (5).

Generation of Intein N-ATP7B Deletion Constructs

The following primer pairs were used to generate the intein N-ATP7B deletion constructs: JB-WND-1A (5′-TGCAGGATCCCATATGCCTGAACAGGAGAGACAGAT-3′), JB-WND-1B (5′-CGTGTCGACTTACACTGCTCTGGTTGATTGTGG-3′), JB-WND-2A (5′-

TGCAGGATCCCATATGGCACCGCAGAAGTGCTTC-3′), and JB-WND-2B (5′-TGCAGTCGACTTAGGCCAGGGAAGCATGAAAGCC-3′). The coding sequences for the intein deletionN-ATP7B constructs were amplified from recombinant pcDNA3.1(+) ATP7B with Pfu DNA polymerase (Invitrogen). Forward primers introduced BamHI and NdeI restriction sites, while reverse primers introduced a SalI restriction site. Consequently, the amplified fragments were digested with NdeI and SalI restriction endonucleases and ligated into the pTYB12 plasmid digested with the same enzymes. The generated N-ATP7B, MBD5–6, MBD1–4, MBD1–4 without a loop, and the chitin binding domain (CBD) were expressed in BL21 cells with the thioredoxin expression plasmid pTx. Soluble lysate was bound to chitin resin (NEB) and phosphorylated as described above for MBP-N-ATP7B. Protein was eluted from resin with sample buffer, and phosphorylation was analyzed by gel electrophoresis as described above for MBP-N-ATP7B.

Expression and Phosphorylation of His-Tagged N-ATP7B in HEK293 Cells

HEK293 cells were seeded to confluency onto six-well plates 24 h before transfection. Cells were transfected with His-tagged N-ATP7B cloned into the pTriEx vector using 4 μg of DNA with 10 μL of Lipofectamine 2000 (Invitrogen, Carlsbad, CA). The medium was changed 6 h post-transfection. For intracellular phosphorylation of expressed His-tagged N-ATP7B, cells were metabolically labeled with inorganic phosphate. Specifically, 24 h after transfection, cells were washed and then incubated for 30 min with phosphate free MEM (Gibco) at 37 °C. Then phosphate free MEM containing 0.1 mCi/mL [^{32}P] orthophosphate was added to the cells and incubated for 3 h. Cells were then scraped, dounce-homogenized in PBS, and centrifuged for 30 min at 20000*g*, and the soluble lysate was incubated with chitin resin (to reduce the nonspecific background at the following step) for 1 h. The unbound fraction was transferred to the cobalt-NTA resin (Sigma) for 1 h to bind His-tagged N-ATP7B. After washes with PBS, containing 20 mM imidazole, 2 mM AEBSF, EDTA free Protease Inhibitor Cocktail, and 0.1% DDM, protein was eluted with PBS, 250 mM imidazole, 2 mM AEBSF, EDTA free Protease Inhibitor Cock-tail, and 0.01% DDM and loaded onto 7.5% Laemmli gels. Gels were transferred onto PVDF (Immobilon-P, Millipore), and membranes were exposed to Kodak BioMax MS film for detection of radioactive bands.

RESULTS

Membrane-Bound ATP7B Is Phosphorylated in Vitro by a Membrane-Bound Kinase

For the initial characterization of ATP7B phosphorylation, we utilized recombinant ATP7B expressed in *Sf9* cells. ATP7B expressed in *Sf9* cells is functional (14) and constitutes ~2% of the total membrane protein. This amount is significantly higher than the levels of endogenous ATP7B in hepatocytes, which simplifies the in vitro analysis. First, we determined whether the membrane-bound human ATP7B could be phosphorylated in vitro using a soluble fraction of human cell lysate (HepG2 or HEK293 cell lysates were used with similar results). Addition of the lysate and radioactive ATP resulted in the appearance of a phosphorylated 165 kDa band (the expected size for ATP7B) in the ATP7B-containing membranes. No such band was observed in control membranes from the mock transfected cells (Figure 2A).

Phosphorylation of ATP7B was also observed using cell lysates from the *Sf9* cells. Unexpectedly, even in the absence of cell lysate, the membrane-bound ATP7B was efficiently phosphorylated (Figure 2A). Membranes from HepG2 cells, containing endogenous ATP7B, also exhibited phosphorylation of ATP7B in the absence of cell lysate (not shown). Altogether, these results suggested that either ATP7B is phosphorylated by a membrane-associated kinase (which is similar for the insect and mammalian cells) or ATP7B itself may have a kinase activity.

Catalytic Activity of ATP7B Is Not Necessary for a Kinase-Mediated Phosphorylation

ATP7B binds and hydrolyzes ATP in a reaction that invloves a transfer of γ-phosphate from ATP to invariant aspartate D1027 and a formation of a transient acyl–phosphate intermediate (14). (This catalytic intermediate is unstable at basic pH and cannot be detected on a regular Laemmli gel that we use to observe stable kinase-mediated phosphorylation shown in Figure 2A.) To test whether the known ATPase activity of ATP7B is necessary for kinase-mediated phosphorylation (i.e., whether ATP7B itself acts as a kinase), we utilized the D^{1027} A mutant of ATP7B, which lacks the ability to hydrolyze ATP (14). This mutant was phosphorylated (Figure 2B), indicating that the kinase-mediated phosphorylation is unrelated to the known catalytic activity of ATP7B and is rather mediated by a different protein.

To determine whether the kinase was a membrane-bound or a soluble protein recruited by ATP7B from the cytosol, we incubated ATP7B-containing membranes with increasing (from 0 to 1.0 M) concentrations of NaCl, then pelleted membranes, and carried out phosphorylation. Incubation with a high level of salt disrupts weak hydrogen bonding and ionic interactions between proteins, and if the kinase was recruited to the membrane through transient interactions with ATP7B, the salt treatment was expected to disrupt the interactions. However, an only 10–20% decrease in the degree of phosphorylation was observed (not shown), suggesting that the kinase is either a membrane protein or a soluble protein bound to the membrane as a part of a very stable complex.

Properties of the ATP7B Kinase

To gain a better understanding of the kinase activity involved in phosphorylation of ATP7B and further optimize the conditions for kinase-mediated phosphorylation, we characterized the nucleotide and metal ion dependence of the kinase. Using a range of ATP concentrations (50 nM to 700 μM), we determined the apparent K_m of the ATP7B kinase for ATP to be ~50 μM (Figure 3A). GTP can substitute for ATP in some common kinases, such as casein kinase; therefore, we conducted experiments to compare kinase activation by these two nucleotides. The membranes were first incubated with 1.3 pmol of [γ-^{32}P]ATP in the presence and absence of 50 μM GTP. As seen in Figure 3B, the level of phosphorylation was similar. We then increased the total radioactivity to 13.3 pmol of [γ-^{32}P]ATP while keeping the specific activity of ATP the same. We also added either 500 μM cold GTP or 500 μM cold ATP. The increase in the amount of radioactive ATP resulted in a higher degree of phosphorylation of ATP7B, while a large excess of cold GTP was without effect. These results indicate that ATP is a preferred substrate for the ATP7B kinase. Addition of cold ATP showed the expected decrease in the amount of phosphorylation.

Metal Dependence of the Kinase

The dependence on various divalent metals is a common property of cellular kinases. The majority of kinases utilize magnesium as a cofactor for phosphorylation, while some kinases use cobalt. The metals stabilize ATP and/or create hydrogen bonding contacts in the ATP binding pocket. To investigate the metal dependence of the membrane-bound ATP7B kinase in *Sf*9 cells, $MgCl_2$ in the phosphorylation buffer was substituted with either $MnCl_2$, $CoCl_2$, or EDTA (divalent metal chelator) or no metal was added. Magnesium and manganese were found to induce a similar level of phosphorylation (Figure 3C). In the presence of $CoCl_2$, phosphorylation of ATP7B was detected, but at much lower level compared to that with $MgCl_2$ or $MnCl_2$ (Figure 3C). No phosphorylation was observed in the absence of metal.

Proteolysis within the N-Terminal Domain Increases the Level of Phosphorylation of ATP7B

We noticed that in addition to full-length ATP7B (165 kDa protein), a 136 kDa protein, which was absent in mock infected controls, was highly phosphorylated (Figure 2A,B). We

hypothesized that the 136 kDa fragment was generated by proteolysis of the full-length ATP7B. To determine whether proteolysis occurs within the N-terminal or C-terminal region of the protein, we generated and characterized the C-terminally His-tagged variants of ATP7B as well as the ATP7B D^{1027} A mutant. Phosphorylation of these constructs was similar to that of the nontagged ATP7B (data not shown). Solubilization and purification of theHis-taggedATP7B on Ni-NTA resin yielded both the full-length 165 kDa ATP7B and the 136 kDa band (Figure 4A, top panel); subsequent Western blot analysis of fractions further confirmed that the 136 kDa band represents a degradation product of ATP7B (Figure 4A, bottom panel). Since ATP7B was His-tagged at the C-terminus, the retention of the 136 kDa product on the Ni-NTA resin indicates that this product was generated by the removal of the N-terminal 29 kDa fragment.

We attempted to identify the site of proteolytic cleavage by direct amino acid sequencing of the 136 kDa fragment. These experiments were unsuccessful due to either modification of the N-terminus during sample preparation or the presence of several closely spaced cleavage sites (data not shown). On the basis of its size, the 136 kDa fragment lost approximately 260 residues from full-length ATP7B, i.e., the segment that includes MBD1, MBD2, and a part of MBD3 (see the predicted position of the cleavage site in Figure 1).

Densitometry measurements of the protein and scintillation counts of phosphorylated protein for the full-length and 136 kDa fragment bands revealed that the 136 kDa band incorporated ~5 times more phosphate than the full-length ATP7B (Figure 4B). The ATP7B D^{1027} A variant, although less phosphorylated than the wild-type protein, also showed a significant increase in the level of phosphorylation (4-fold) for the 136kDa fragment. These results suggest that the removal of the MBD1–2/3 region increases the level of phosphorylation of ATP7B either by exposing the remaining N-terminus or by unmasking other domains in ATP7B.

The N-Terminal Domain of ATP7B (N-ATP7B) Is a Target of Phosphorylation in Vitro and in Vivo

To determine whether N-ATP7B is a target of phosphorylation or only regulates the access of the kinase to other domains, it was important to determine the location of phosphorylation sites in ATP7B. It was previously shown that ATP7B is phosphorylated on serine residues (15). The ATP7B sequence contains 126 serines; this large number excludes site-directed mutagenesis as an efficient strategy for the identification of phosphorylation site(s). To identify the sites of phosphorylation, we digested the purified, in vitro phosphorylated ATP7B and identified the peptides by mass spectrometry. Phosphopeptides were not detected, due to either low abundance or low peptide coverage [only ~30% of the full-length ATP7B sequence was covered by identified peptides for any given experiment (data not shown)].

Consequently, to narrow the location of the phosphorylation region, three major cytosolic domains of ATP7B were considered: the C-terminal domain, the ATP-binding domain (ABD), and N-ATP7B. The C-terminal domain is known to contain signals for the trafficking of ATP7B; however, the deletion of the C-terminal tail does not prevent the phosphorylation of ATP7B in mammalian cells (10). Both ABD and N-ATP7B have a number of potential sites for kinase-mediated phosphorylation. These domains were expressed as fusion proteins, purified, and used in the in vitro phosphorylation assay using mammalian cell lysate as a source of a kinase. ABD was phosphorylated minimally above background (data not shown), while N-ATP7B repeatedly showed a significant level of phosphorylation that was dependent on incubation with the lysate (Figure 5A). These results suggested that in vitro, N-ATP7B was a target of a kinase-mediated phosphorylation.

To verify that N-ATP7B is a physiologically relevant substrate, we measured the level of N-ATP7B phosphorylation in cells. The His-tagged N-ATP7B was expressed in human HEK293

cells, metabolically labeled with the orthophosphate (^{32}P), and purified on Co-NTA resin. Autoradiography of purified protein showed that it was labeled with phosphate (Figure 5B). No phosphorylated band was found in the immunoprecipitates from the mock transfected cells. Interestingly, in addition to the 70 kDa band, corresponding to the size of N-ATP7B, we observed an additional 100 kDa band (that was also absent in a mock), suggesting that the phosphorylated N-ATP7B may form a complex with some other protein. Altogether, we concluded that the N-ATP7B is a target for the kinase-mediated phosphorylation in vivo and in vitro.

Copper Binding to N-ATP7B Facilitates Phosphorylation by a Copper-Independent Kinase

It was previously shown that the phosphorylation of ATP7B in cells is regulated by copper (10); however, it was not apparent whether copper binding to N-ATP7B made ATP7B a better substrate for the kinase or the kinase itself was copper-dependent. Our in vitro assay for phosphorylation of N-ATP7B provided a convenient method for differentiating between these two possibilities. For these studies, we used purified N-ATP7B maltose binding protein fusion (MBP-N-ATP7B) that was expressed in *Escherichia coli*. MBP-N-ATP7B can be loaded with copper in a cell, and the subsequent in vitro additions of copper during the kinase assay are not necessary (13).

First, we determined whether the intensity of phosphorylation of N-ATP7B depended on copper binding to this domain. Second, we tested whether the level of phosphorylation increases when the lysates for the phosphorylation assay were prepared from cells that had been exposed to 50 μM copper chloride for 1 h before cell lysis. If the kinase had to be activated by copper or some copper-dependent factor, then the copper-treated lysate should phosphorylate N-ATP7B more efficiently. Figure 6 illustrates that copper-bound MBP-N-ATP7B has higher level of phosphorylation compared to that of apo-MBP-N-ATP7B. Phosphorylation with copper-treated lysate did not increase the level of phosphorylation, compared to that of basal lysate (for either the apo or copper-bound MBP-N-ATP7B). Thus, the copper-bound status of N-ATP7B affects the level phosphorylation of ATP7B, while the kinase activity appears to be independent of copper.

Copper Induces Rearrangements of Loops Connecting MBDs

It was previously shown that copper binding to N-ATP7B was accompanied by structural changes (7); however, the nature of these changes has not been determined. To improve our understanding of structural consequences of copper-dependent rearrangements that facilitate phosphorylation, we prepared apo and copper-bound MBP-N-ATP7B and carried out limited proteolysis under conditions that were optimized for cleavage only in exposed linker regions between MBDs (8). This step was followed by 2D gel electrophoresis and analysis of the peptide maps (Figure 7). The pattern of tryptic digest fragments for apo and Cu-bound protein was significantly different. Cu-bound N-ATP7B exhibited only three intense spots in the mass region below 16 kDa (the region of masses for individual MBDs and MBD pairs), while 10 distinct spots could be identified for the apo form. Fewer low-molecular weight fragments for Cu-N-ATP7B is indicative of a rearrangement of MBD loops and an overall “structural tightening” of the N-terminal domain upon copper binding.

Identification of low-molecular weight peptides (<16 kDa) derived from the apo-N-ATP7B (Table 1) revealed that together their sequences cover the entire length of N-ATP7B. Specifically, we detected individual domains MBD1 and MBD2, MBD2 as a pair with MBD3, and MBD5 as a pair with MBD6. These results indicate that several linker regions, specifically loops MBD1–2, MBD2–3, and MBD4–5, were exposed and available for proteolysis.

Only three peptides in the ≤ 16 kDa mass region were visible for the copper-bound form of N-ATP7B. However, a new peptide at 23 kDa that was absent in the apo-ATP7B digest pattern (Figure 7) was detected. Two major spots in the low-molecular weight region contained MBD3. Compared to the MBD3-containing peptides in the apo-N-ATP7B digest, the peptides identified from the copper-N-ATP7B map were considerably shorter [~8 kDa compared to 13 and 16 kDa; with a lower pI (see Table 1)]. Thus, copper binding results in a structural rearrangement and better exposure and digestion of the MBD2–3 linker region (for predicted cleavage sites, see Table 1). The third spot was identified as thioredoxin, which most likely copurified with N-ATP7B. The peptide quantities contained in other spots were insufficient for identification by LC-MS.

Because the two most intense spots for apo-N-ATP7B included the individual MBD2 and MBD3 regions while the only identified peptides in Cu-N-ATP7B were from MBD3, we concluded that another major conformational change upon copper binding is occurring within the MBD1–2 region. This change results in a lower level of exposure or an increased level of structure in this region. In contrast, upon copper binding the loop following MBS3 remains exposed and is cleaved.

The Sites of Phosphorylation Are Located in the Loop between MBS3 and MBS4

For further mapping, the N-ATP7B in a copper-bound form was phosphorylated in vitro and then subjected to limited proteolysis with trypsin. The phosphorylated peptides were separated by a 2D gel (Figure 8), transferred onto PVDF, exposed to film, and then further digested with trypsin, eluted, and identified by tandem mass spectroscopy (Table 2). The majority of the label was found in two spots in the 23 kDa region (Figure 8). All peptides recovered from these spots belonged to the MBD3–6 region (Table 2), indicating that the C-terminal half of N-ATP7B was the target of phosphorylation. The mobility and identity of peptides are also consistent with the predicted map of all possible tryptic fragments (phosphorylated and nonphosphorylated) that can be generated under our conditions considering that the loop regions are long and can be cleaved in several positions (see Figure 1 of the Supporting Information). The presence of two major spots similar in mass but different in charge suggested that more than one site in the 23 kDa fragment was phosphorylated.

To further narrow the region of phosphorylation, we generated and examined phosphorylation of several deletion variants of N-ATP7B tagged to a chitin-binding domain (CBD) (Figure 9). Unexpectedly, chitin resin showed a higher background (several non-ATP7B bands, which originated from the cell lysate, were detected). Nevertheless, it was apparent that the N-ATP7B variants, including the MBD1–4 region, were phosphorylated (independently of whether the loop connecting MBD4 and MBD5 was present), while the fragment including MBD5–6 was not. No phosphorylation of the CBD tag was detected (negative control). Altogether, the results of mass spectrometry of phosphorylated spots (showing peptides from the MBD3–6 region) and limited proteolysis (showing phosphorylation of the MBD1–4 fragment) pointed to the linker between MBD3 and MBD4 as a target of phosphorylation.

DISCUSSION

An appropriate level of intracellular copper is determined by the metabolic needs of individual cells, while the activity of Cu-ATPases is required to balance these levels. The Cu-ATPases are regulated by phosphorylation in response to changes in copper concentration, and this modification is coupled to intracellular localization of the transporters. We demonstrate that this regulatory modification involves kinase activities, in the cytosol and at the membrane. The data presented here allow for two scenarios: phosphorylation of ATP7B by two different kinases or phosphorylation by a kinase that is soluble (Figure 5) but can be recruited to the

membrane to form a stable complex with either ATP7B or proteins in the proximity of ATP7B (Figure 2).

Previously published data suggested that basal phosphorylation of ATP7B occurs in the absence of the N-terminal domain, while for the copper-dependent phosphorylation, the N-terminus is needed (10). It is possible that the membrane-bound kinase activity is required for basal phosphorylation (and perhaps for retention of ATP7B in the TGN), while soluble kinase phosphorylates N-ATP7B, when it binds copper. Either kinase activity is Mg^{2+}-dependent and does not appear to be stimulated by copper. This latter observation suggests that conformational changes in ATP7B and not copper sensing by a kinase represent a likely trigger for phosphorylation of ATP7B and trafficking. This conclusion is supported by an earlier report that some ATP7B mutants can traffic from the TGN in the absence of high levels of copper (16). Phosphorylation of ATP7B may serve as a signal for trafficking by facilitating interaction with the components of the cellular trafficking machinery.

Our data illustrate that N-ATP7B is the target for the kinase-dependent phosphorylation in vitro and in vivo. Binding of copper elicits conformational changes within the domain and leaves most of the loop less accessible to proteolysis. By contrast, theMBD3–4 loop remains exposed as evidenced by the presence of MBD3 as one of only very few peptides in the 2D map of Cu-bound N-ATP7B (Figure 7). It is this loop that appears to be phosphorylated by a kinase in a copper-bound state ofN-ATP7B (the summary of events is shown in Figure 1). The increase in the level of phosphorylation of recombinant N-ATP7B that we observed in vitro (25–30%) is lower than the 2–3-fold increase that we reported for full-length ATP7B in cells (10). This difference could be due to interactions between N-ATP7B and ABD in full-length ATP7B (8). Such interaction may hinder access to phosphorylation site(s) in the N-ATP7B, markedly decreasing the background level of phosphorylation. This is in contrast to the copper-bound state when domains dissociate and the phosphorylation site, presumably, becomes more exposed. In isolated N-ATP7B, no such restrictions exist and phosphorylation proceeds in both the apo and copper-bound forms.

In conclusion, we have developed a reliable in vitro phosphorylation assay for ATP7B and N-ATP7B and demonstrated that N-ATP7B is a direct target of kinase-mediated copper-dependent phosphorylation. Our findings suggest that copper binding results in significant rearrangement of N-ATP7B, thereby facilitating access and phosphorylation of sites within the MBD3–4 region. We suggest that the structural changes within N-ATP7B represent a sensory mechanism that regulates posttranslational modification of ATP7B and possibly trafficking. The developed assays can be utilized for isolation and further identification and characterization of the ATP7B kinase.

Acknowledgments

We thank Dr. Ashley McCormack and Dr. Larry David for help with the mass spectroscopy experiments and Dr. Burkhead for generating the MBD1–4 expression constructs.

REFERENCES

1. Bartee MY, Lutsenko S. Hepatic Copper-Transporting ATPase ATP7B: Function and Inactivation at the Molecular and Cellular Level. Biometals 2007;20:627–637. [PubMed: 17268820]
2. Guo Y, Nyasae L, Braiterman LT, Hubbard AL. NH2-Terminal Signals in ATP7B Cu-ATPase Mediate Its Cu-Dependent Anterograde Traffic in Polarized Hepatic Cells. Am. J. Physiol 2005;289:G904–G916.
3. Roelofsen H, Wolters H, Van Luyn MJ, Miura N, Kuipers F, Vonk RJ. Copper-Induced Apical Trafficking of ATP7B in Polarized Hepatoma Cells Provides a Mechanism for Biliary Copper Excretion. Gastroenterology 2000;119:782–793. [PubMed: 10982773]

4. Hung IH, Suzuki M, Yamaguchi Y, Yuan DS, Klausner RD, Gitlin JD. Biochemical Characterization of the Wilson Disease Protein and Functional Expression in the Yeast *Saccharomyces cerevisiae*. J. Biol. Chem 1997;272:21461–21466. [PubMed: 9261163]
5. Lutsenko S, Barnes NL, Bartee MY, Dmitriev OY. Function and Regulation of Human Copper-Transporting ATPases. Physiol. Rev 2007;87:1011–1046. [PubMed: 17615395]
6. Lutsenko S, Leshane ES, Shinde U. Biochemical Basis of Regulation of Human Copper-Transporting ATPases. Arch. Biochem. Biophys 2007;463:134–148. [PubMed: 17562324]
7. Didonato M, Hsu HF, Narindrasorasak S, Que L Jr, Sarkar B. Copper-Induced Conformational Changes in the N-Terminal Domain of the Wilson Disease Copper-Transporting ATPase. Biochemistry 2000;39:1890–1896. [PubMed: 10677240]
8. Tsivkovskii R, Macarthur BC, Lutsenko S. The Lys1010-Lys1325 Fragment of the Wilson's Disease Protein Binds Nucleotides and Interacts with the N-Terminal Domain of This Protein in a Copper-Dependent Manner. J. Biol. Chem 2001;276:2234–2242. [PubMed: 11053407]
9. Huster D, Lutsenko S. The Distinct Roles of the N-Terminal Copper-Binding Sites in Regulation of Catalytic Activity of the Wilson's Disease Protein. J. Biol. Chem 2003;278:32212–32218. [PubMed: 12794172]
10. Vanderwerf SM, Cooper MJ, Stetsenko IV, Lutsenko S. Copper Specifically Regulates Intracellular Phosphorylation of the Wilson's Disease Protein, a Human Copper-Transporting ATPase. J. Biol. Chem 2001;276:36289–36294. [PubMed: 11470780]
11. Voskoboinik I, Fernando R, Veldhuis N, Hannan KM, Marmy-Conus N, Pearson RB, Camakaris J. Protein Kinase-Dependent Phosphorylation of the Menkes Copper P-Type ATPase. Biochem. Biophys. Res. Commun 2003;303:337–342. [PubMed: 12646208]
12. Lowry OH, Rosebrough NJ, Farr AL, Randall RJ. Protein Measurement with the Folin Phenol Reagent. J. Biol. Chem 1951;193:265–275. [PubMed: 14907713]
13. Lutsenko S, Petrukhin K, Cooper MJ, Gilliam CT, Kaplan JH. N-Terminal Domains of Human Copper-Transporting Adenosine Triphosphatases (the Wilson's and Menkes Disease Proteins) Bind Copper Selectively in Vivo and in Vitro with Stoichiometry of One Copper per Metal-Binding Repeat. J. Biol. Chem 1997;272:18939–18944. [PubMed: 9228074]
14. Tsivkovskii R, Eisses JF, Kaplan JH, Lutsenko S. Functional Properties of the Copper-Transporting ATPase ATP7B (the Wilson's Disease Protein) Expressed in Insect Cells. J. Biol. Chem 2002;277:976–983. [PubMed: 11677246]
15. Vanderwerf SM, Lutsenko S. The Wilson's Disease Protein Expressed in Sf9 Cells Is Phosphorylated. Biochem. Soc. Trans 2002;30:739–741. [PubMed: 12196182]
16. Cater MA, La Fontaine S, Mercer JF. Copper Binding to the N-Terminal Metal-Binding Sites or the Cpc Motif Is Not Essential for Copper-Induced Trafficking of the Human Wilson Protein (ATP7B). Biochem. J 2007;401:143–153. [PubMed: 16939419]
17. Walker JM, Huster D, Ralle M, Morgan CT, Blackburn NJ, Lutsenko S. The N-Terminal Metal-Binding Site 2 of the Wilson's Disease Protein Plays a Key Role in the Transfer of Copper from Atox1. J. Biol. Chem 2004;279:15376–15384. [PubMed: 14754885]

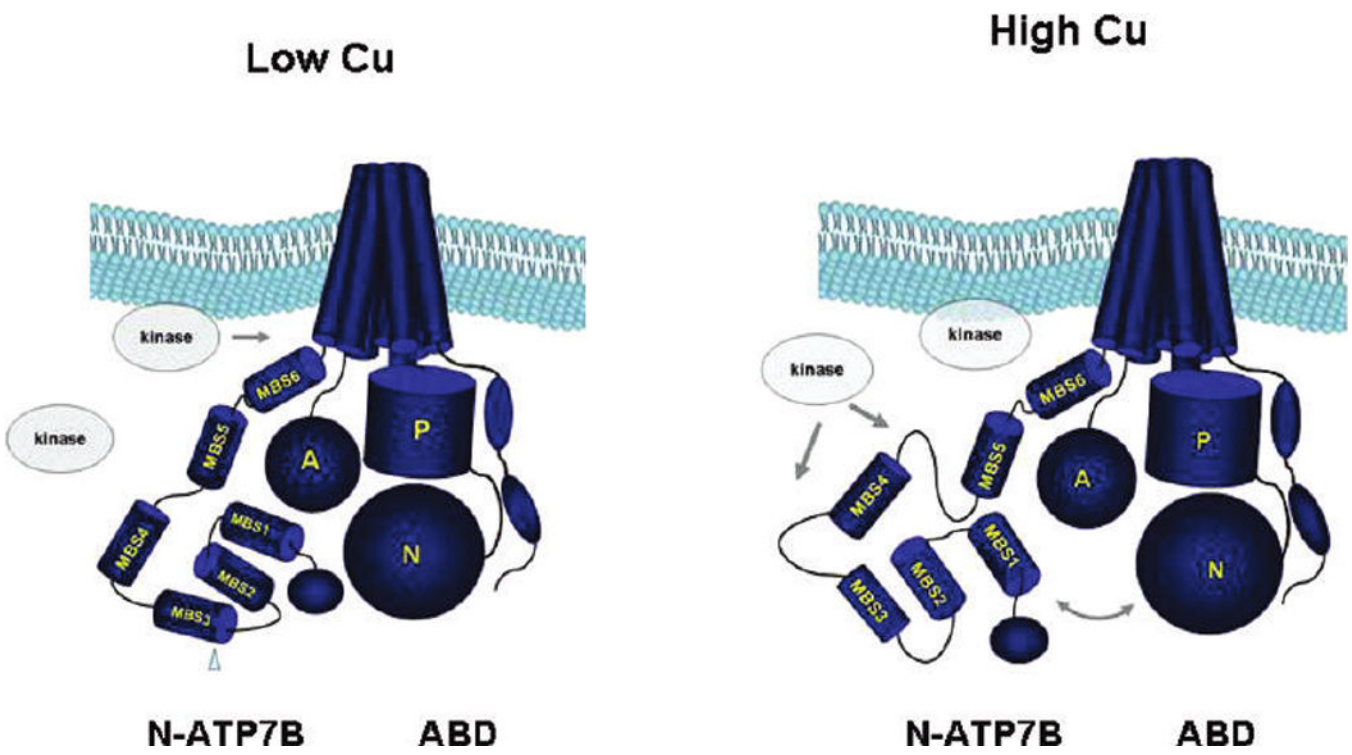

FIGURE 1.

Model of the domain organization of ATP7B at low and high copper levels. The N-terminal domain of ATP7B (N-ATP7B) consists of six metal-binding subdomains (MBS1–6) and in its apo form interacts with the ATP-binding domain (ABD), which in turn is composed of the N-domain and P-domain. At low levels of copper, ATP7B is basally phosphorylated by a kinase. We described in this study that when copper binds to N-ATP7B (high level of copper), the accompanying structural changes in N-ATP7B result in exposure of additional sites for kinase-mediated phosphorylation (for further details, see text). The predicted position of proteolytic site(s) that removes the 29 kDa fragment is indicated with a triangle. The kinase (s) phosphorylating ATP7B can be present in the membrane and in the cytosol.

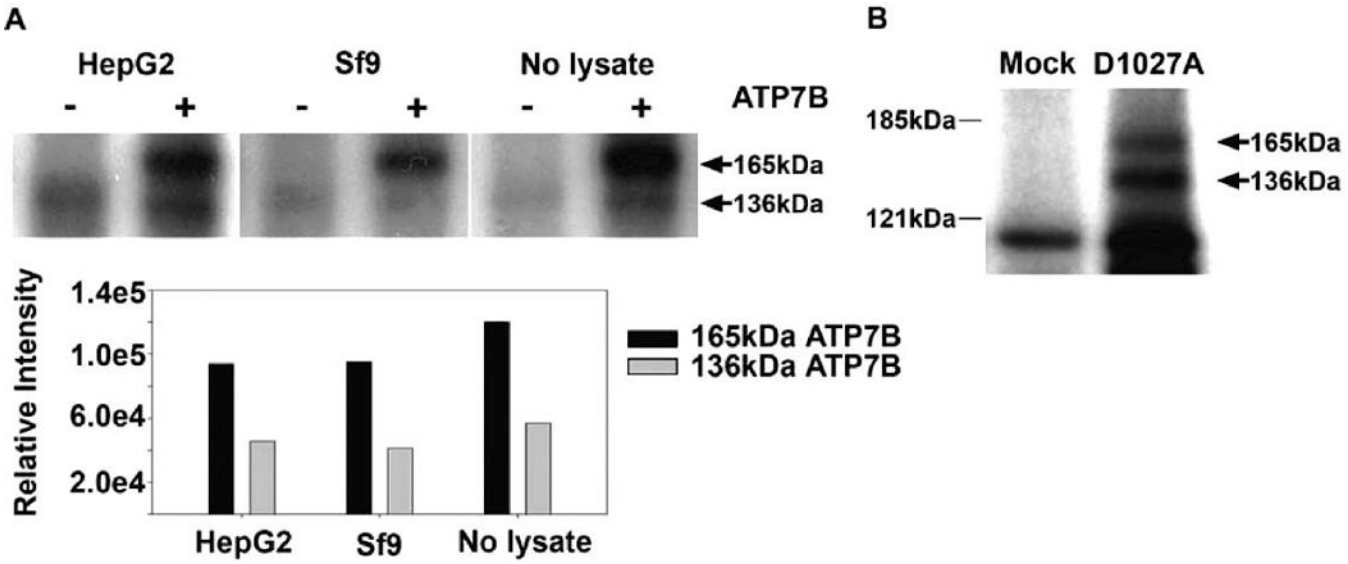

FIGURE 2.

Recombinant ATP7B can be phosphorylated in vitro by a membrane-bound kinase. (A) Control (−) or ATP7B-containing (+) membranes from *Sf9* cells were phosphorylated in the presence or absence of soluble lysate from mammalian (HepG2) or insect (*Sf9*) cells. Arrows indicate the full-length ATP7B and the 136 kDa product. The relative intensities of the bands are graphed below. (B) Microsomal membrane fractions were prepared from *Sf9* cells infected with the empty virus (Mock) or with the virus expressing the ATP7B D^{1027} A mutant and phosphorylated in vitro with [γ-^{32}P] ATP. Equal amounts of membrane protein were separated with a Laemmli gel, dried, and analyzed by autoradiography. The arrows indicate the position of full-length (165 kDa) and proteolyzed (136 kDa) ATP7B.

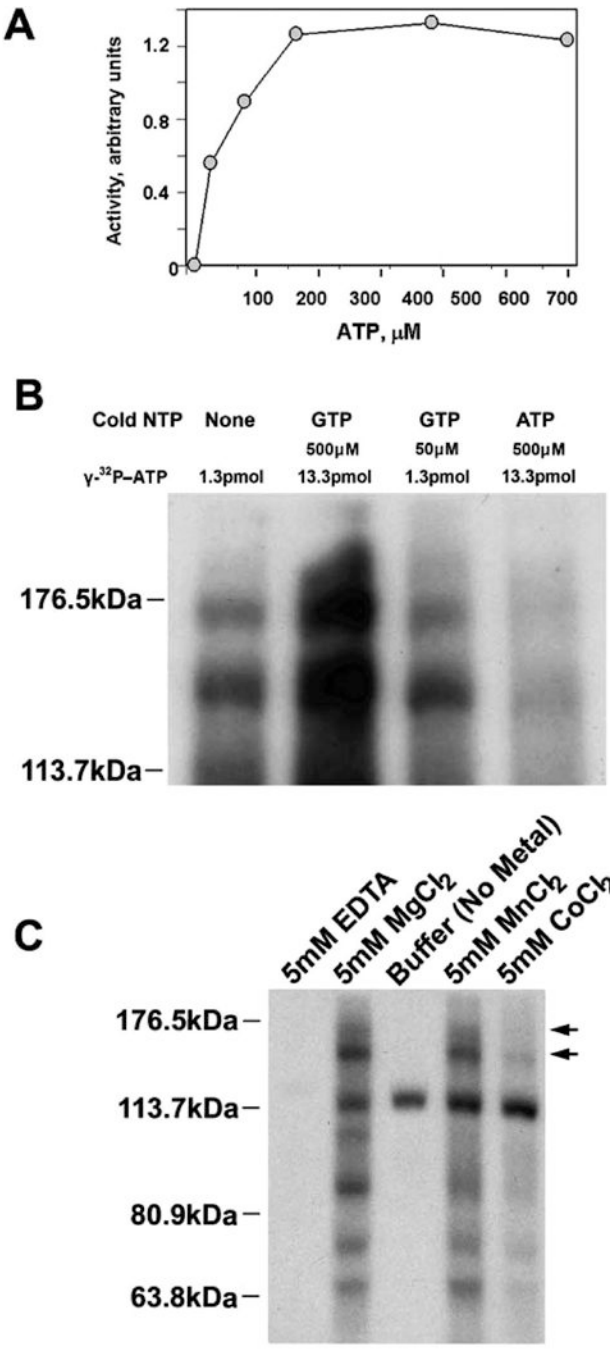

FIGURE 3.

Characterization of ATP7B kinase. (A) A range of ATP concentrations was used to optimize phosphorylation conditions. The half-maximum phosphorylation was observed at ~50 μM, and 100 μM ATP was used in subsequent phosphorylation experiments. A representative experiment is shown. (B) Nucleotide specificity of the kinase. The phosphorylation was examined with two different amounts of [γ-^{32}P]ATP (1.3 or 13.3 pmol) in the presence of excess cold nucleotide (50 and 500 μM GTP or 500 μM ATP as a control). At either concentration of ATP, excess GTP was without effect, indicating that ATP is a preferred substrate. (C) Metal dependence of the ATP7B kinase. Membranes were phosphorylated in the

absence (no additions or EDTA) or presence of 5 mM divalent metal. Arrows indicate the positions of ATP7B and the 136 kDa product.

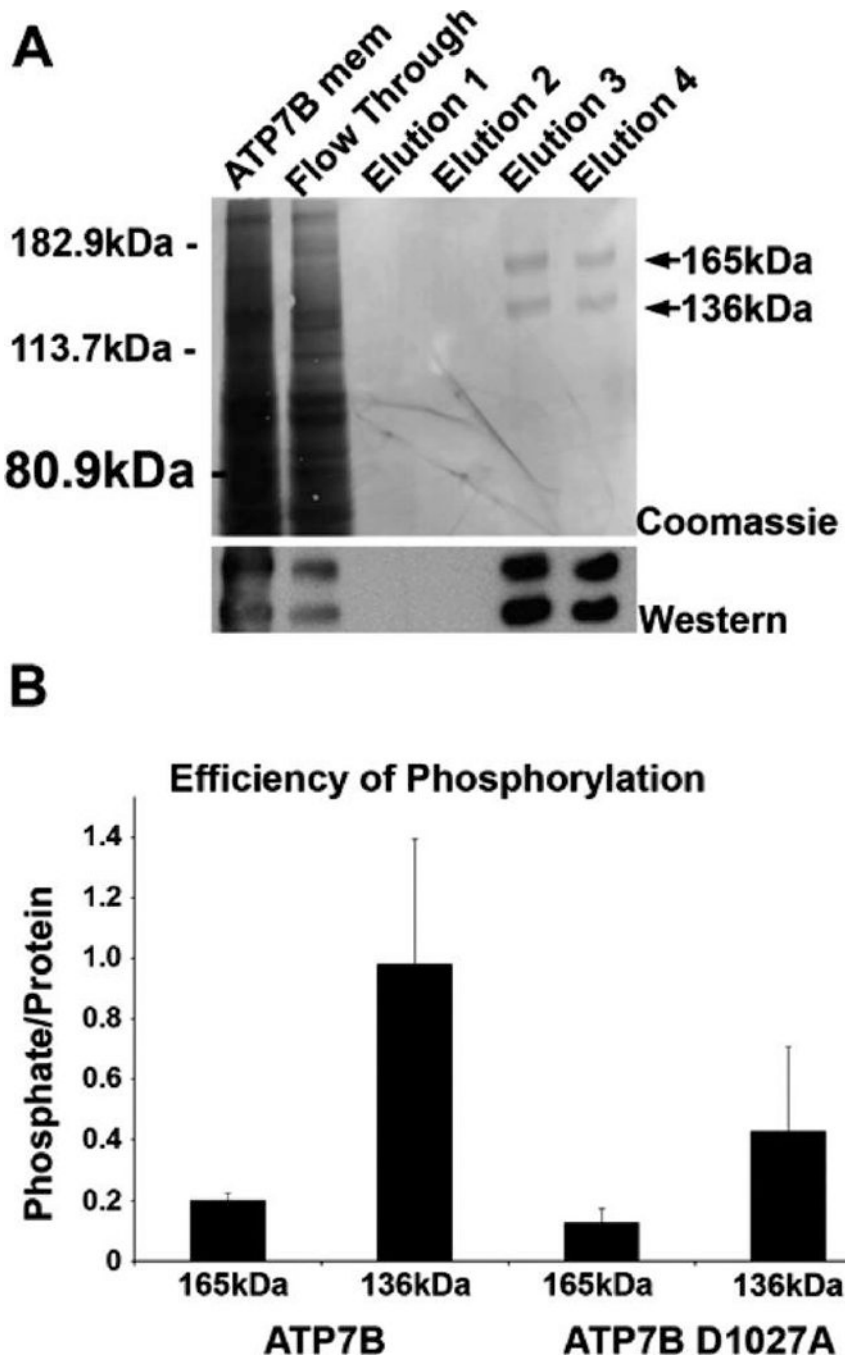

FIGURE 4.

ATP7B product (136 kDa) that lacks the N-terminus and has a higher level of phosphorylation. (A) A C-terminal His-tagged ATP7Bwas expressed in *Sf9* cells as described above. Solubilized full-length ATP7B and the 136 kDa degradation product can both be purified on Ni-NTA resin: top panel, Coomassie staining of purified protein; bottom panel, Western blot showing the 165 and 136 kDa products are recognized by the anti-ATP7B antibody. (B) Quantitation of the efficiency of phosphorylation (phosphate to protein) for 165 kDa/136 kDa ATP7B and the ATP7B D^{1027} A mutant by scintillation counts.

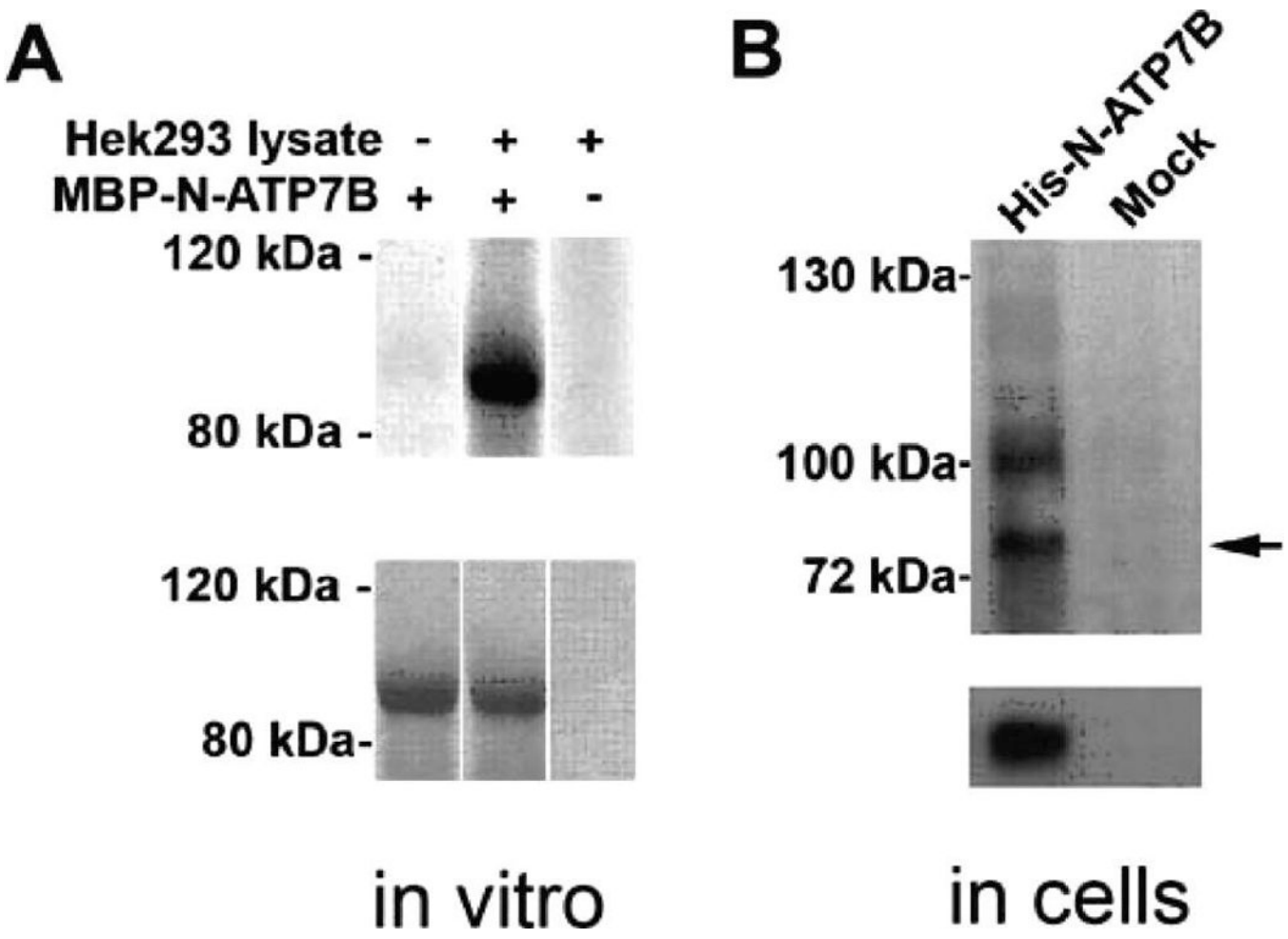

FIGURE 5.

N-ATP7B is a target of phosphorylation in vitro and in cells. (A) MBP-N-ATP7B was bound to a amylose resin and phosphorylated with the HEK293 cell lysate: top panel, autoradiography; bottom panel, Coomassie staining. (B) To confirm phosphorylation of N-ATP7B in vivo, HEK293 cells were transfected with the Histagged N-ATP7B and metabolically labeled with orthophosphate (^{32}P): top panel, autoradiography; bottom panel, Western blot with anti-N-ATP7B antibody.

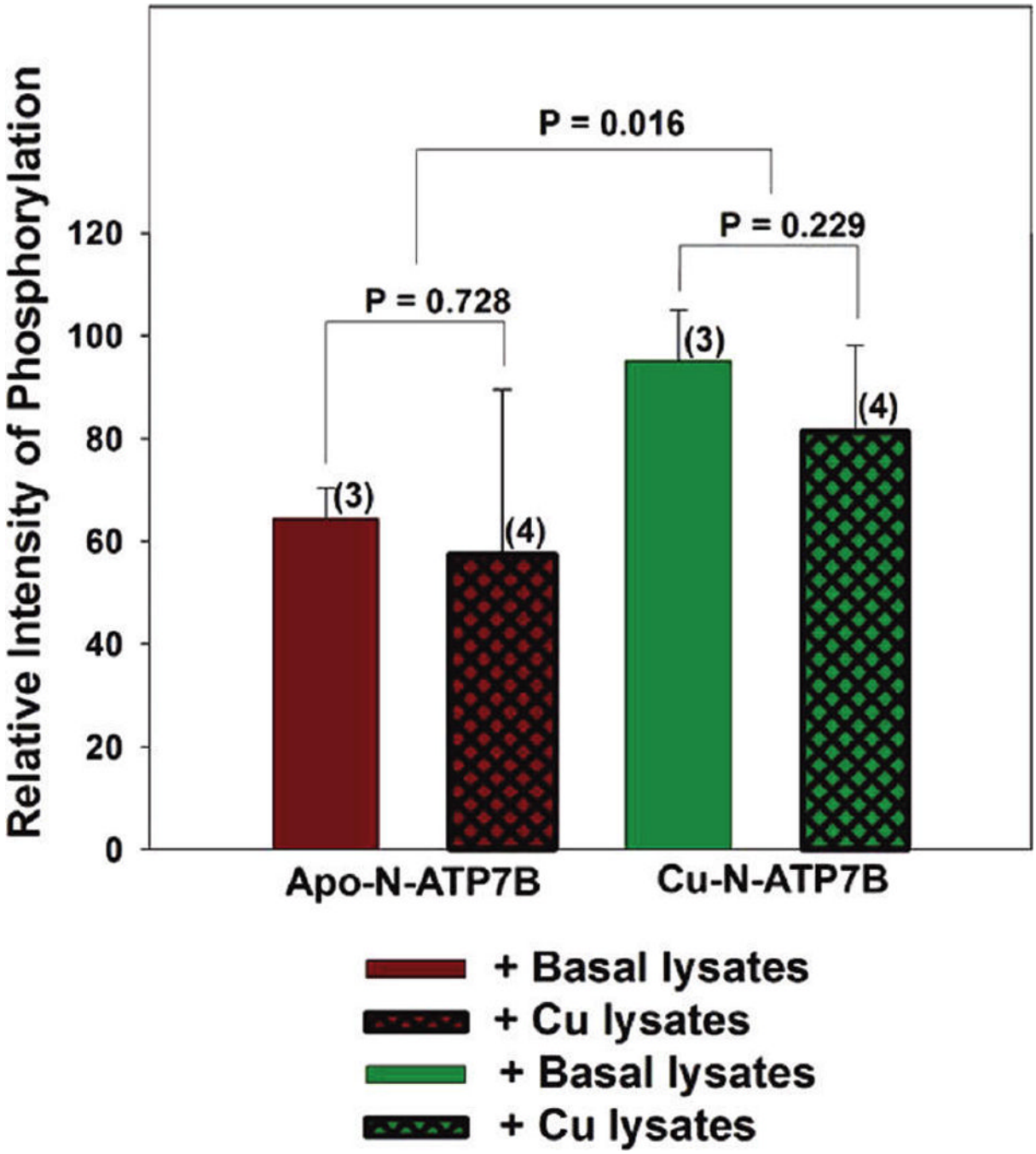

FIGURE 6.

Effect of copper on phosphorylation of MBP-N-ATP7B by a soluble kinase. MBP-N-ATP7B (expressed and purified in either the apo form or the copper-bound form) was incubated with the lysates from control HEK293 cells or cells treated with 50 μM copper chloride for 1 h before cell lysis. Copper-bound N-ATP7B shows a higher level of phosphorylation, while lysates from control and copper-treated cells yielded similar levels of phosphorylation.

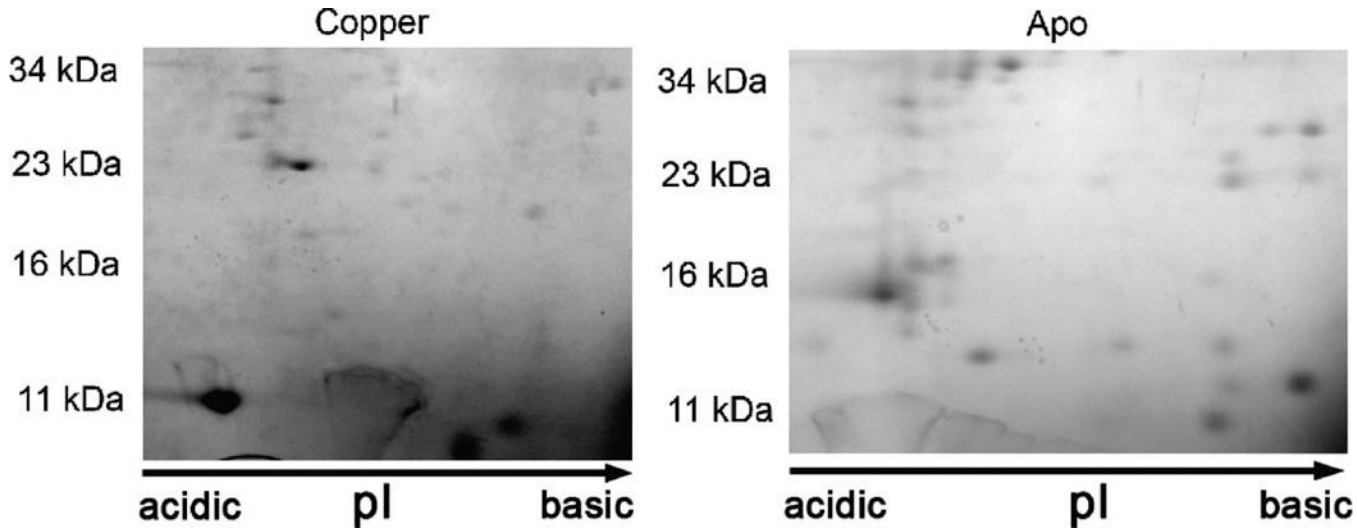

FIGURE 7.

Copper alters the accessibility of loops connecting MBDs to proteolysis. 2D gel electrophoresis of the partially digested apo-MBP-N-ATP7B (left) and Cu-bound MBP-N-ATP7B (right). Spots below the 16 kDa region were excised and identified by LC-MS (MBP is not cleaved under these conditions and runs as a 42 kDa protein).

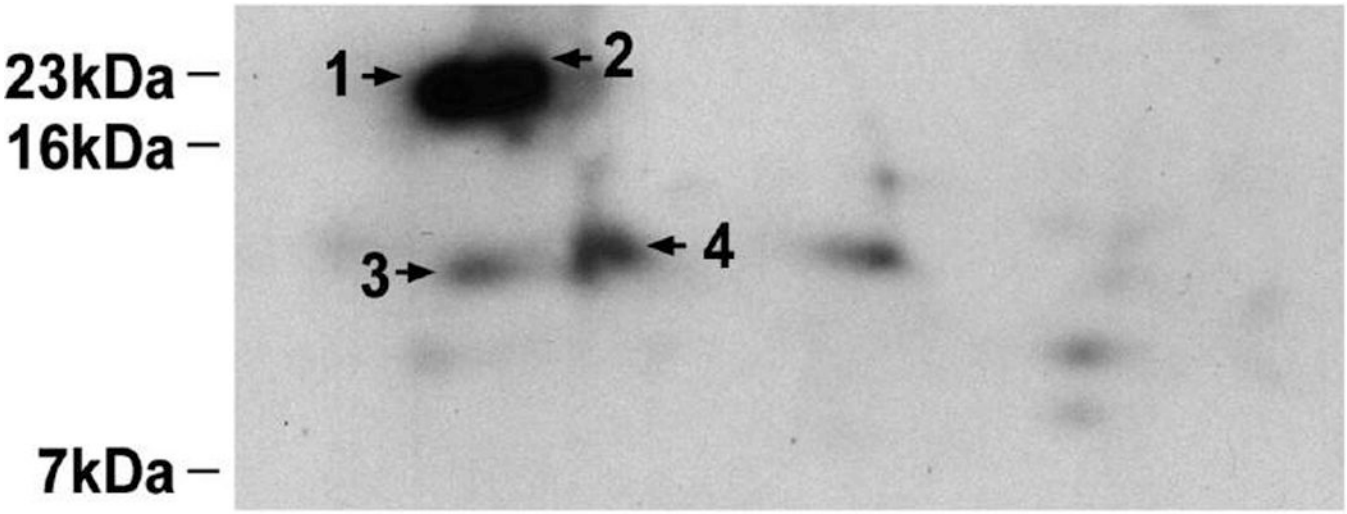

FIGURE 8.

Localization of the region of phosphorylation toMBD3–6 of N-ATP7B. To narrow the region of phosphorylation, labeled Cu-bound N-ATP7B was proteolyzed with trypsin for 3 h, and the peptides were separated on a 2D gel. The phosphorylated spots were analyzed by LC-MS. Arrows indicate identified spots.

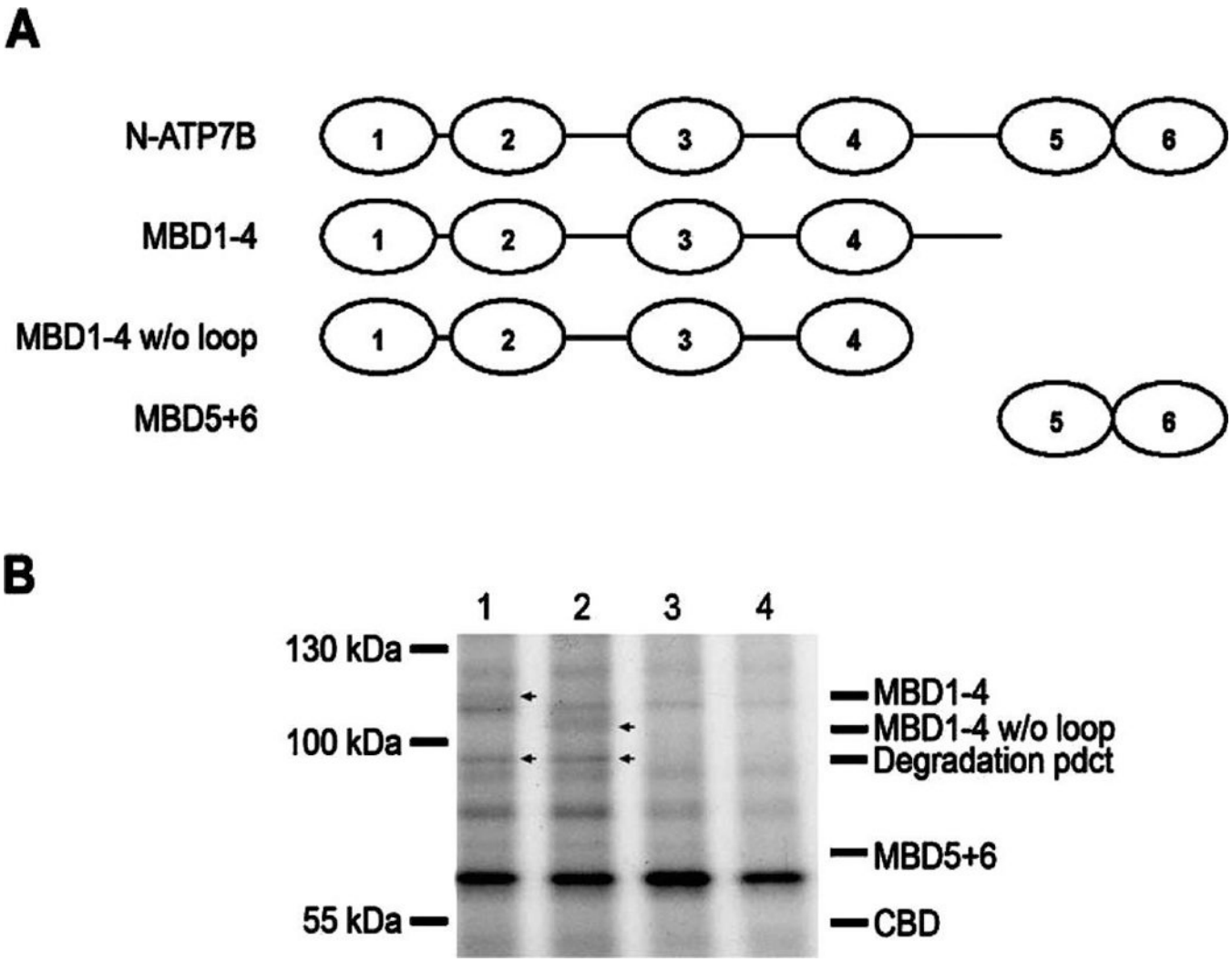

FIGURE 9.

Phosphorylation region located in loop 3, between MBD3 and MBD4. (A) Deletion variants of N-ATP7B used for phosphorylation. (B) Proteins expressed and phosphorylated on a chitin resin using cell lysate and [γ-^{32}P]ATP; the lysate was removed, resin washed, and phosphorylated protein eluted with sample buffer and analyzed by gel electrophoresis: lane 1, MBD1–4; lane 2, MBD1–4 without a loop; lane 3, MBD5–6; lane 4, CBD.

Table 1

Proteolytic Peptides in the 6–16 kDa Region Generated from Apo and Copper-Bound N-ATP7B

spot	M_w (Da)	pI	amino acid residues	metal binding site[d]	relative intensity
			Apo Form		
1[a]	9874	5.2	36–129	L0-MBD1	10
2[b]	14866	5.2	478–620	L4-MBD5-MBD6	30
3[b]	16319	5.8	176–324	MBD2-MBD3	20
4[b]	10074	6.1	17–129	L0-MBD1	10
5[b]	13495	6.1	214–339	L2-MBD3-L3	80
6[a]	8302	6.5	137–211	MBD2	10
7[a]	13660	6.5	199–324	MBD2-L2-MBD3	100
8[a,c]	16506	5.3	466–603	L4-MBD5-L5	100
9[b]	16147	6.1	199–339	MBD2-L2-MBD3	20
11[b]	15691	5.0	478–623	MBD5-MBD6	20
			Cu-Bound Form		
1	11806	4.7	Thioredoxin		100
2[b]	8177	5.1	263–339	M3-L3	40
3[b]	8470	5.5	270–351	M3-L3	40

[a] Beginning and ending peptides were identified.

[b] Peptides identified by LC–/MS were included in a sequence to match the molecular weight and the pI of the spot.

[c] Spot identified from an earlier gel.

[d] MBD, metal-binding domain; L, linker region.

Table 2

Sequences of Peptides within Phosphorylated Spots and Their Location within N-ATP7B

spot	peptide	region
1	407 VISPEELR	MBD4
	439 HSAGNSMVQTTDGTPTSVQEVAPHTGR	loop 4
	466 LPANHAPDILAK	loop 4
	589 TNGITYASVALATSK	MBD6
2	352 NQVQGTCSTTL	loop 3
	340 SSSSHSPGSPPR	loop 3
	415 AAIEDMGFEASVVSESCSTNPLGNHSAGN	MBD4
	444 SMVQTTDGTPTSVQEVAPHTGR	loop 4
	466 LPANHAPDILAK	loop 4
	496 GMTCASCVSNIER	MBD5
	512 EAGVLSVLVALMAGK	MBD5
	595 ASVALATSK	MBD6
	608 FDPEIIGPR	MBD6
3	512 EAGVLSVLVALMAGK	MBD5
	589 TNGITYASVALATSK	MBD6
	608 FDPEIIGPR	MBD6
4	314 AIEALPPGNFK	MBD3
	270 SCVLNIEENIGQLLGVQSIQVSLENK	MBD3